ORIGINAL ARTICLE

Challenges of relief modeling in flat areas: a case study in the Amazon coast floodplains

Leonardo Nogueira dos Reis[1] - ORCID: 0000-0002-3826-7179

Laurent Polidori[1,2] - ORCID: 0000-0001-6220-9561

[1] Universidade Federal do Pará, Instituto de Geociências, Programa de Pós-Graduação em Geologia e Geoquímica, Belém - Pará, Brazil.
E-mail: leo2reisgeo@gmail.com, laurent.polidori@ufpa.br

[2]Centre d'Etudes Spatiales de la Biosphère, CESBIO, Toulouse, France.
E-mail: laurent.polidori@ird.fr

Abstract:

This study aimed to evaluate the performance of eight digital elevation models (DEMs), i.e., one digital terrain model (DTM) obtained from airborne P-band radar (BCDCA DTM), one digital surface model (DSM) obtained from airborne X-band radar (BCDCA DSM) and six DSMs from orbital sensors (AW3D30, ASTER GDEM, Copernicus DEM, NASADEM, SRTM, Topodata), for the morphological characterization of the floodplains of Amapá (Brazil). All DEMs were resampled to the same mesh size and compared by visual and statistical analysis in terms of elevation and slope. The comparison demonstrated that the DTM obtained from P-band radar images was the most consistent one in representing the landforms, as it is less sensitive to vegetation. The behavior of the automated hydrographic network extraction was also analyzed, showing that even the DTM was not able to detect drainage lines across flat landscapes with centimeter elevation variations. As the comparisons were made with a common 30 m grid, the conclusions are limited to this scale and the effect of a change of scale is discussed. In view of the difficulty of automatically extracting the network in a plain, the possibility to reduce the modelling to a 2D approach, based on external hydrographic data, is also discussed.

Keywords: Digital elevation model; Digital terrain model; P-band radar; Floodplains; Amazon.

1. Introduction

Digital elevation models (DEM) consist in the digital representation of elevation values at different points of a specific geographical area, such as the Earth's topography or the objects located on it (Polidori and El Hage 2020; Guth et al. 2021). The numerous possibilities of analyses derived from these products (e.g., slope maps, watershed analyses, flood modeling) have made them widely applied in geosciences, especially in terms of local terrain descriptors (Valeriano et al. 2006; Colby and Dobson 2010; Clubb et al. 2017). From the altimetry of a DEM, it is possible to generate numerical interpretations of the relief, such as slope, vertical and horizontal curvatures and shading relief maps. These products may be generated through the interpolation of contour lines on topographic maps or the processing of digital images obtained by satellite, airplane or drone.

The most widely used imaging techniques are photogrammetry, based on optical stereoscopic image pairs, and radar interferometry (InSAR), based on the processing of two radar echoes backscattered by the same surface (Zebker and Goldstein 1986). Another way to acquire elevation data is through Lidar (Light detection and ranging), a high-precision active sensor that obtains the distance of objects on surface by measuring the propagation time of laser beams (Wehr and Lohr 1999). The use of these products requires a clear definition of the physical surface to be modeled, since the term is generic, and represents any surface with altimetric values. A digital surface model (DSM) results from techniques where the signal is reflected by the forest canopy or by other objects above the ground surface, as obtained by most DEM production techniques, such as photogrammetry and short-wavelength radar interferometry (Polidori and El Hage 2020; Guth et al. 2021). A digital terrain model (DTM) represents the ground surface and is usually obtained from GNSS field surveys, topographic contour maps, Lidar, as well as long-wavelength InSAR, which is capable of penetrating the forest canopy (Polidori et al. 2018).

The scarcity of cartographic bases is one of the main obstacles to studies of the Amazon relief, with most of the knowledge coming from the RADAM project, carried out with airborne radar at a 1:1,000,000 scale (Azevedo 1971; Van Roessel and Godoy 1974). Due to an extensive vegetation cover, few access roads and extended periods of cloudiness, the region is challenging for field campaigns and even for analyses using remote sensing, especially with optical sensors. Although some DEMs are designed to overcome these obstacles, the modeled surface needs to be explicitly specified, since the presence, or absence, of vegetation can compromise their interpretation. As the main products freely and globally available are generated from short-wavelength radar and are, therefore, unable to penetrate the forest canopy, most of the errors in the recognition of terrain morphometry in plains are related to a reduced altimetric amplitude, since the height variation in these areas is mostly related to noise or vegetation cover. This issue does not exist in mountainous areas, where the altimetric amplitude is larger than the non-topographic variability. In floodplains, DEMs can also have ambiguities in specifying the surface to be surveyed, e.g., an area that is flooded for a period of the year, where the reference surface can be either the soil, the vegetation or the water. As a result, a correct definition of the drainage network for hydrographic analysis can be impaired (Polidori, El Hage and Valeriano 2014; Zingaro et al. 2021).

The quality of a DEM can be assessed by comparing it into a reference DEM, a common approach in the literature (Hayakawa, Oguchi and Lin 2008; Grohmann 2018; Pham et al. 2018), or by evaluating its shape realism, based on visual control and quantitative geomorphometry (Valeriano et al. 2006; Polidori and El Hage 2020). This work aims to compare the performance of different DEMs (global, national and local) in the morphological characterization of a floodplain area, considering possible morphometric limitations in representing the landforms of flat and floodable regions with dense vegetation cover, as the Amazon Coastal Zone. The comparison is based on the assumption that the water surface is horizontal and the floodplain tends to be horizontal, so that any feature that is not horizontal is not topographical (mainly vegetation). Improvement strategies are also proposed to enhance these products in similar areas, so the interpretations derived from them be closer to the reality that their users intend to achieve.

2. Study area

The Amazon Coastal Zone (ACZ) is marked by high temperatures (above 20°C) with low annual thermal variation, high precipitation rate (above 2,000 mm/year) and cloudiness (Nittrouer, Brunskill and Figueiredo 1995; Santos 2006). It comprises the coastal strip from the Orinoco Delta, in Venezuela, to the São Marcos Bay, in Maranhão, and presents several humid environments, such as beaches, tidal plains, salt and sweet marshes, estuaries, mangroves, lowland and upland forests, lagoons, and islands (Figure 1B; Souza Filho et al. 2005; Santos 2006). The study area is located in Brazil, at the southern portion of the Amapá State coast, in the city of Mazagão (Figure 1A). The area varies in elevation from 0 to 55 meters, with the highest region located at the northwest side and the lowest to the southeast, towards the Amazon River.
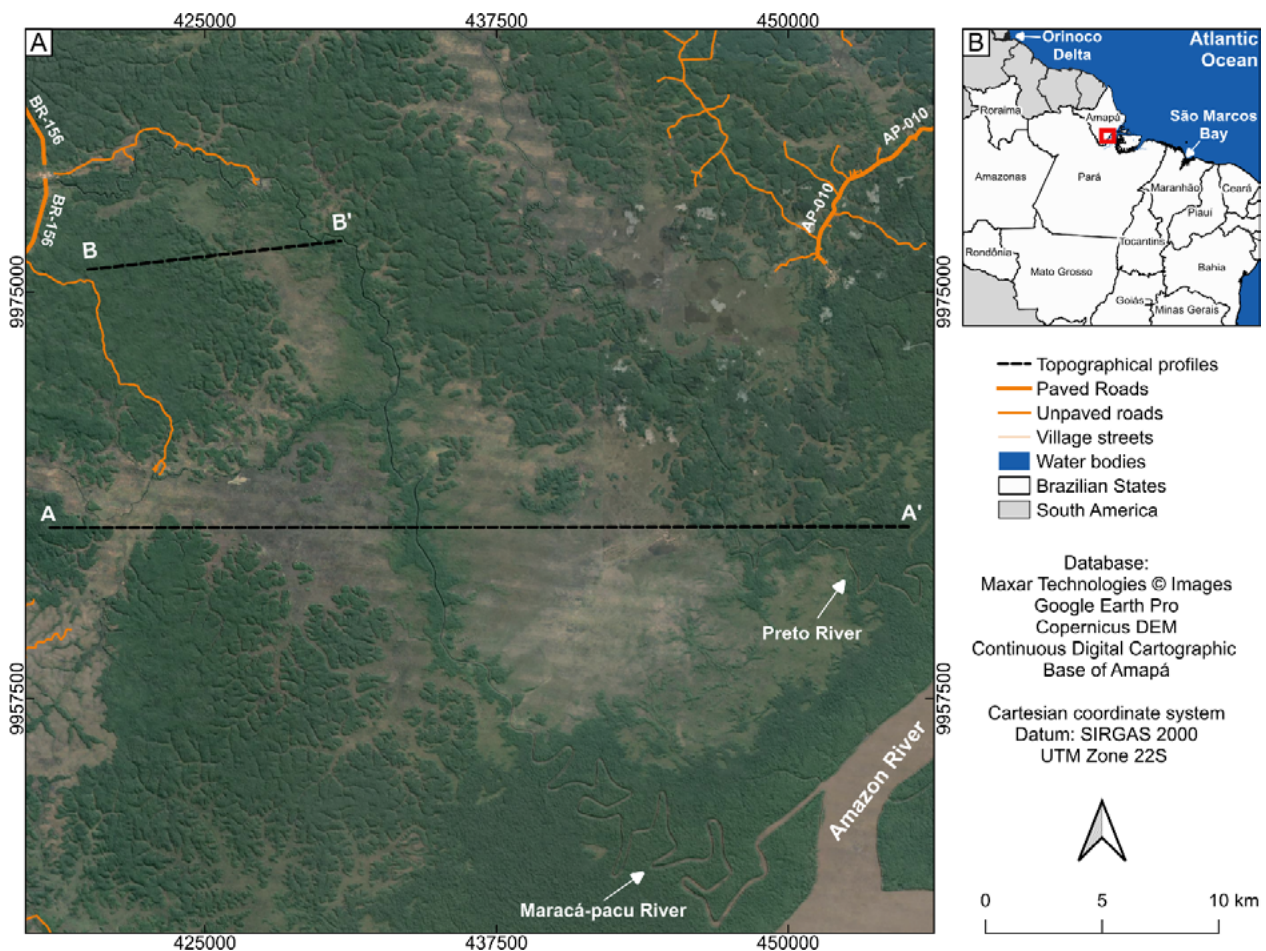

Figure 1: A) Overview of the study area with the topographic profiles that were analyzed; B) Location of the study area (red frame).

In Amapá State, the coastal zone extends for about 350 km from the mouth of the Amazon River towards the sea. Besides being located in the largest equatorial forest on the planet, it receives direct influence from the discharge of the Amazon River and its main tributaries, and is conditioned to a regime of strong currents and macro-tides with amplitudes of up to 12 m (Santos 2006; Santos et al. 2008; Pereira et al. 2009). Its coastal plain comprises a range of Quaternary sediments of fluvial, fluvio-lacustrine and fluvio-marine environments, and an extensive range of plateaus (Silveira 1998; Silveira and Santos 2006). These environments are formed by sandy-clay and sandy to conglomeratic sediments, with the presence of lateritic concretions (Silveira 1998). The local

geomorphology is characterized by a flat relief, subject to constant reworking by erosion and accretion processes, where meteorological, fluvial and coastal processes (tidal flooding) favor the formation of floodplains (Torres and El-Robrini 2006).

The dominant vegetation classes are lowland forests, upland forests, herbaceous and shrub lands, and savanna (Rabelo 2008). The lowland forests are located on the banks of the Amazon River estuary and inside of the rivers that drain the coastal plain, being subject to a daily cycle of floods and ebbs related to the tides, with species that reach up to 20 m in height (Santos 2006). The upland forest is characterized by higher structure species (above 25 m), associated with low plateau and submontane environments (Rabelo 2008). Herbaceous and shrub lands are part of the floodplain of the rivers and estuaries that drain the region and are found between the floodplain forest units and the limit of the coastal plain, with a tidal flooding regime (Santos 2006). The savanna is marked by strong climatic and pedological gradients, campestris vegetation with scattered woody flora and a dissected low plateau relief (Rabelo 2008).

The weather and climate conditions in the ACZ are controlled by one of the most important meteorological systems acting in the tropics, the Intertropical Convergence Zone (ITCZ). The influence of ITCZ on the ocean surface temperature and, consequently, the convergence of humidity, creates conditions that favor the formation of rain clouds. Therefore, the region presents two distinct seasons during the year (Figure 2), a rainy one (with extreme precipitation events generating large-scale flooding on the coast) and a dry one (Souza and Cunha 2010).
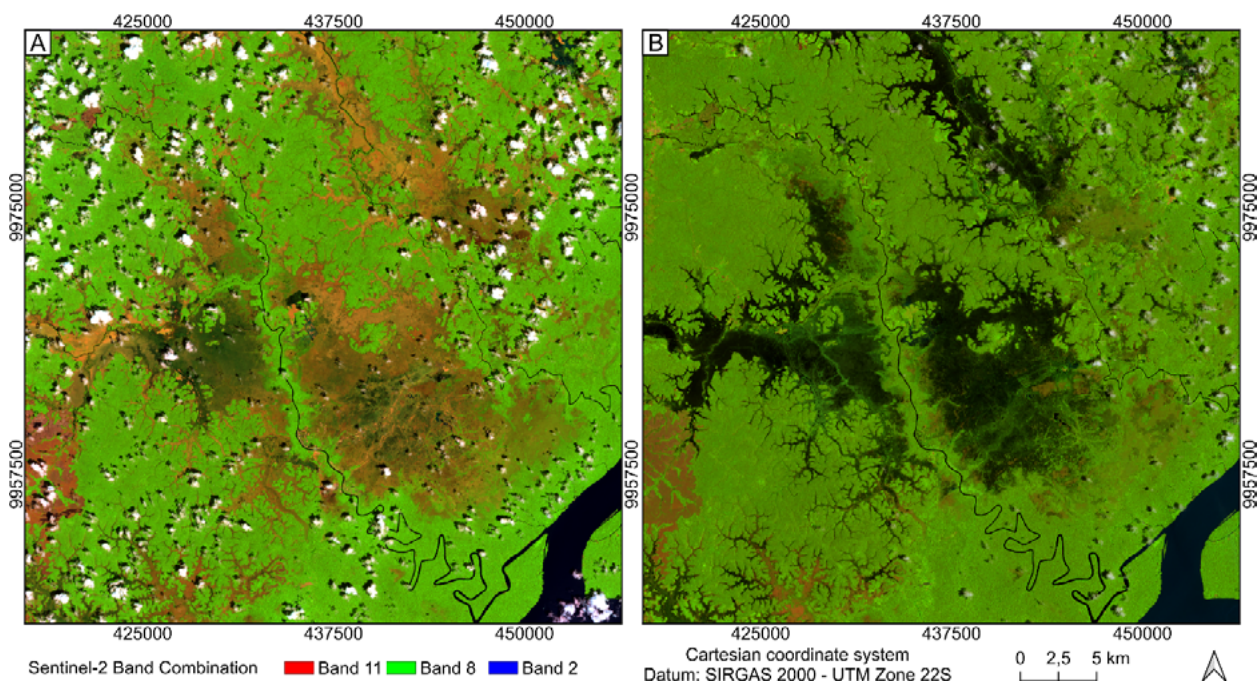

Figure 2: Sentinel-2 images (R11G8B2). A) dry season (Oct/2021); B) rainy season (Feb/2020).

3. Materials and methods

3.1 Elevation Data

Eight digital elevation models were analyzed (Table 1). Two of these models are part of the Continuous Digital Cartographic Base of Amapá (BCDCA), a set of geospatial information generated over the whole Amapá State

from airborne InSAR in P and X bands. It includes a series of by-products, such as BCDCA DTM (P-band), BCDCA DSM (X-band) and vectorized data (e.g., hydrographic network). This database was produced by the Directorate of Geographical Services of the Brazilian Army and made available by the Amapá State Environment Secretariat (Vieira 2015). The availability of a DTM that covers its entire territory makes Amapá a unique case in the world for topographic analysis in forested areas, one of the reasons for choosing this study area.

Six DSM obtained from orbital imaging were also selected. Four of them derived from orbital missions using InSAR techniques (Copernicus DEM, NASADEM, SRTM V3 and Topodata) and two of them, AW3D30 and ASTER GDEM, were generated from orbital photogrammetry, using stereoscopic images from the PRISM (Panchromatic Remote-Sensing Instrument for Stereo Mapping) and the ASTER (Advanced Spaceborne Thermal Emission and Reflection Radiometer) sensors, respectively (Tachikawa et al. 2011; Takaku et al. 2014). NASADEM, SRTM and Topodata were derived from the same data obtained from the Shuttle Radar Topography Mission, whose primary objective was mapping the topography of continental areas between 60°N and 54°S by InSAR in C and X bands (Farr et al. 2007). NASADEM is the most recent version, with improved processing techniques and data from other products to minimize voids and extend the spatial coverage (Buckley et al. 2020). Topodata is a 30 m grid refinement of the first 90 m grid SRTM dataset obtained by kriging over the Brazilian territory, with the intention to represent the surface with consistency of its angular properties between neighboring cells (i.e., slope, orientation, etc.), an important factor in geomorphometric analysis (Valeriano and Rossetti 2012).

Table 1: Digital elevation models of global, national, and local scope used in this work.

DEM	Method	Spatial resolution	Acquisition Period	Horizontal accuracy (RMSE)	Vertical accuracy (RMSE)	Source
ALOS WORD 3D (AW3D30) V3.1	Orbital photogrammetry	1.0 arcseg (~30 m)	2006-2011	5 m	5 m	Takaku et al. (2014)
ASTER GDEM V3	Orbital photogrammetry	1.0 arcseg (~30 m)	2011	30 m	20 m	Tachikawa et al. (2011)
BCDCA DTM	P-band airborne InSAR	0.08 arcseg (~2.5 m)	2014	< 7,5 m	3,33 m (bare soil) 4,56 m (forest areas)	SEMA-AP (2015)
BCDCA DSM	X-band airborne InSAR	0.08 arcseg (~2.5 m)	2014	< 7,5 m	3,33 m	SEMA-AP (2015)
COPERNICUS DEM	X-band orbital InSAR	1.0 arcseg (~30 m)	2011-2015	< 6 m	< 4 m	Leister-Taylor et al. (2020)
NASADEM	SRTM V3 reprocessing	1.0 arcseg (~30 m)	2000	< 20 m	< 16 m	Buckley et al. (2020)
SRTM V3	C and X-band orbital InSAR	1.0 arcseg (~30 m)	2000	< 20 m	< 16 m	Farr et al. (2007)
TOPODATA	SRTM V1 kriging refinement	1.0 arcseg (~30 m)	2000	< 20 m	< 16 m	Valeriano and Rossetti (2012)

3.2 Comparative Evaluation of the DEMs

The DEMs were evaluated based on statistical and graphical criteria related to the shape realism of each selected model (Polidori and El Hage 2020). The statistical similarities and differences between them were assessed

for the entire study area on 30 m meshes. This analysis was based on the calculation of Pearson correlation coefficients between the eight DEMs for elevation and slope values, where the closer to 1 is the result between the DEMs, more similar they are with respect to the corresponding morphometric variable (Equation 1).

$$r = \frac{n \left(\sum xy \right) - \left(\sum x \right) \left(\sum y \right)}{\sqrt{[n \sum x^2 - (\sum x)^2] [n \sum y^2 - (\sum y)^2]}}$$ (1)

* x and y: collected values from two different variables; n: number of measures; and r: value between -1 and 1.

As for the differences, all DSMs were compared to the BCDCA DTM, according to equation 2, in order to highlight the influence of vegetation and other artifacts and how they impact in the relief modelling. Since there were no field measurements available, the DTM is used as ground truth.

$$Dx = X_{DEM} - X_{REF}$$ (2)

*DX: difference of variable X (elevation or slope); XDEM: value in the DEM; and XREF: value in the reference model.

The evaluation of DEMs shape realism aims to define how well they preserve the angular properties of the terrain, i.e., slope and azimuth. The models were visually compared based on their hypsometric representation for the whole area, and a detailed visual analysis was made for a small lowland area, using a shape-sensitive shading visualization method to highlight the behavior of each DEM, especially concerning the influence of noise and vegetation cover. They are further tested in a classic geomorphological analysis: the hydrographic network extraction. The results should be reliable in regions where the water runoff is channeled along valleys, but in lowland regions, the extraction algorithm should be much more sensitive to artifacts (noise, vegetation, resampling effect, etc.) and to its own assumptions, such as calculating slope in some privileged directions. All DEMs are compared to a reference, i.e., the official hydrography of Amapá, available in the BCDCA (Vieira 2015). The DEMs were also analyzed in terms of elevation and slope using profiles over a representative axis of different landscapes (low plateau to lowland), to show the impact of vegetation cover on the relief and how it behaves at different scales.

The analyses were processed using GRASS GIS tool package, version 7.8.7, with QGIS Desktop viewer, version 3.22.5 (Grass Development Team 2022; QGIS Development Team 2022). In the statistical evaluation, the *r.covar* command was used to generate a pixel-by-pixel correlation matrix among the DEMs, while the subtraction of the DSMs by the BCDCA DTM was done with QGIS Raster Calculator function. The morphometric variables were generated with *r.slope.aspect* command, while the resampling to different meshes was done based on the *r.resample.interp* command, using the nearest neighbor algorithm. The profile visualization of elevation and slope data was generated with QGIS Terrain Profile plugin. The *Hillshade* function was used to visualize the relief with an illumination azimuth of 30° and an illumination elevation of 45°. For the hydrological analysis, the GRASS GIS *r.stream* toolkit was used. With *r.stream.extract* function, flow networks were extracted from accumulation maps on 30 m meshes. The Multiple flow Direction FD8 algorithm (Holmgren 1994) was used and a value of 100 was set as a criterion in the "Minimum flow accumulation per network" category. The results are transformed into vectors with *r.to.vect* function. All the assessment steps can be seen in Figure 3.
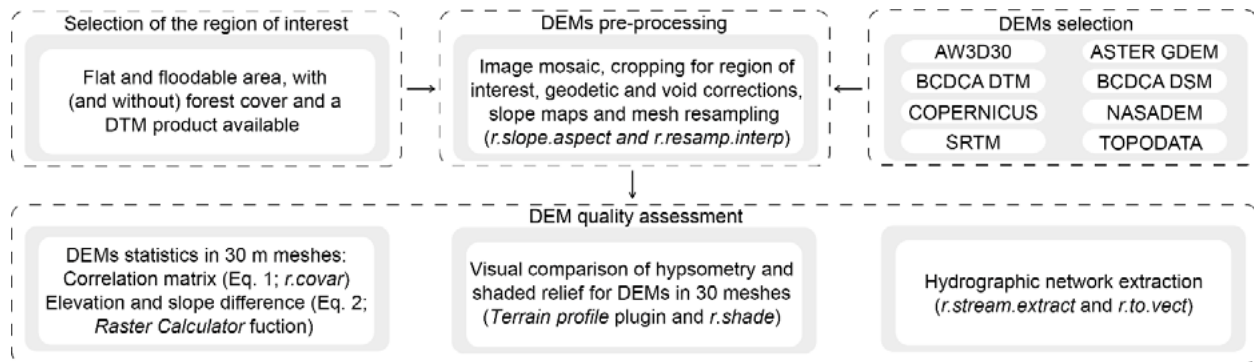
Figure 3: Flowchart of DEM quality assessment steps.

4. Results

The similarity between the selected models was evaluated by correlating their elevation and slope values (Table 2). High elevation correlations are observed between DSMs (above 0.9), except the ASTER GDEM. The NASADEM and SRTM DSMs show the highest correlations (0.986), an expected result, since they use the same input data. Although derived from SRTM, Topodata is mostly correlated to the AW3D30 model (0.975). The BCDCA DSM, which may be considered as the reference DSM for the study area, shows the highest correlation with the Copernicus model. This may be due to the fact that the data acquisitions were carried out at similar periods of time (2014-2015). It was expected that the BCDCA DTM would have the lowest correlation (~0.80), however, the ASTER GDEM presents an even lower correlation (~0.72).

Table 2: Correlation matrix for the eight DEMs resampled at 30 m for elevation and slope.

Elevation	AW3D30	ASTER GDEM	BCDCA DTM	BCDCA DSM	COPERNICUS	NASADEM	SRTM	TOPODATA
AW3D30	1	0.727	0.792	0.946	0.958	0.979	0.978	0.975
ASTER DEM	0.727	1	0.638	0.711	0.722	0.738	0.737	0.719
BCDCA DTM	0.792	0.638	1	0.779	0.803	0.817	0.796	0.796
BCDCA DSM	0.946	0.711	0.779	1	0.970	0.940	0.945	0.930
COPERNICUS	0.958	0.722	0.803	0.970	1	0.958	0.956	0.948
NASADEM	0.979	0.738	0.817	0.940	0.958	1	0.986	0.969
SRTM	0.978	0.737	0.796	0.945	0.956	0.986	1	0.961
TOPODATA	0.975	0.719	0.796	0.930	0.948	0.969	0.961	1
Slope	**AW3D30**	**ASTER GDEM**	**BCDCA DTM**	**BCDCA DSM**	**COPERNICUS**	**NASADEM**	**SRTM**	**TOPODATA**
AW3D30	1	0.213	0.442	0.647	0.652	0.805	0.779	0.707
ASTER DEM	0.213	1	0.122	0.183	0.184	0.229	0.233	0.187
BCDCA DTM	0.442	0.122	1	0.399	0.410	0.450	0.421	0.428
BCDCA DSM	0.647	0.183	0.399	1	0.797	0.652	0.630	0.510
COPERNICUS	0.652	0.184	0.410	0.797	1	0.651	0.627	0.555
NASADEM	0.805	0.229	0.450	0.652	0.651	1	0.814	0.645
SRTM	0.779	0.233	0.421	0.630	0.627	0.814	1	0.648
TOPODATA	0.707	0.187	0.428	0.510	0.555	0.645	0.648	1

For slope, the same relation is observed, but with lower correlation values. The correlation of BCDCA DTM with most DSMs is low (~0.42), due to the high slope values of the upper vegetation surface, while the DTM describes the topography surface with very low slope values in floodplains. The errors seen in ASTER GDEM are more impactful in terms of slope than elevation (0.122). NASADEM and SRTM present the highest correlation for slope (0.814), while Topodata presents a lower correlation compared to the other SRTM related products (~0.64). This occurs due to the kriging resampling used for the model generation to accentuate its angular properties, which acts precisely in the slope values (Valeriano and Rossetti 2012).

The difference in height and slope between each model and BCDCA DTM is reported in Table 3. In both cases, even though AW3D30 and ASTER GDEM show the highest minimum and maximum differences from the terrain reference, AW3D30 has a standard deviation similar to the other DSMs, while ASTER GDEM has the highest standard deviation (10.1 m in elevation and 5.1° in slope), followed by the BCDCA DSM. For elevation, the standard deviation ranges between 7.5 and 7.9 m, while for slope, the DEMs generated from the SRTM mission got slightly better results. Topodata presents the lowest standard deviation values, both for elevation and slope, when compared to the ground reference (7.5 m and 2.2°, respectively).

Table 3: Statistical analysis of the difference in elevation (in meters) and slope (degrees) of the analyzed DEMs using the BCDCA DTM model as reference.

Elevation	Minimum	Maximum	Average	Median	Standard deviation
AW3D30	-22	77	9.3	10	7.9
ASTER GDEM	-24	108	15.9	15	10.1
BCDCA DSM	0	45	11.8	13	8.8
COPERNICUS	-11	40	9.2	10	7.9
NASADEM	-14	40	7.8	8	7.7
SRTM	-12	44	9.7	10	7.8
TOPODATA	-11	41	9.8	10	7.5
Slope	**Minimum**	**Maximum**	**Average**	**Median**	**Standard deviation**
AW3D30	-13	45	2.0	2	2.7
ASTER GDEM	-15	54	4.0	3	5.1
BCDCA DSM	-14	30	3.2	2	4.0
COPERNICUS	-14	27	2.5	1	3.6
NASADEM	-12	25	2.1	2	2.6
SRTM	-13	26	2.3	2	2.7
TOPODATA	-15	16	1.4	1	2.2

With the generation of histograms, it was possible to have a general understanding of the homogeneity of elevation and slope in the study area and of how the models represent these variations. The histograms of the differences between the DSMs and the reference DTM show a bimodal behavior for elevation with a peak around 15-20 m (Figure 4A), and significant slope differences of up to 10° (Figure 4B), both mainly due to the vegetation cover.
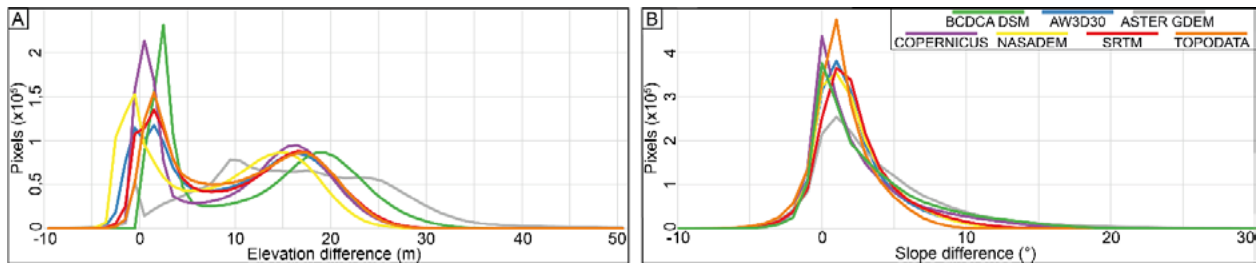
Figure 4: Difference between the DSMs and the DTM, in terms of: A) elevation and B) slope.

The visual comparison between the DEMs confirms the statistical analysis in a more intuitive way. A clear contrast is observed between BCDCA DTM and the other products, especially along the banks of the Amazon River, where the effect of the canopy appears in the surface models generated by photogrammetry or short wavelength radar (Figure 5A). The models with the greatest divergence from the others were AW3D30 (Figure 5C) and ASTER GDEM (Figure 5D), with perceptible noise in the lowland areas. This problem is mainly related to the model generation method (photogrammetry), which is sensitive to the presence of clouds, to the date difference between image acquisitions and to the surface texture that can interfere the stereo matching. As this region is subject to frequent and extensive flooding, the flood area varies between the time series, so the models do not make a correct delineation of water surfaces. This creates artifacts in ASTER GDEM, compromising the distinction between lowland and upland.
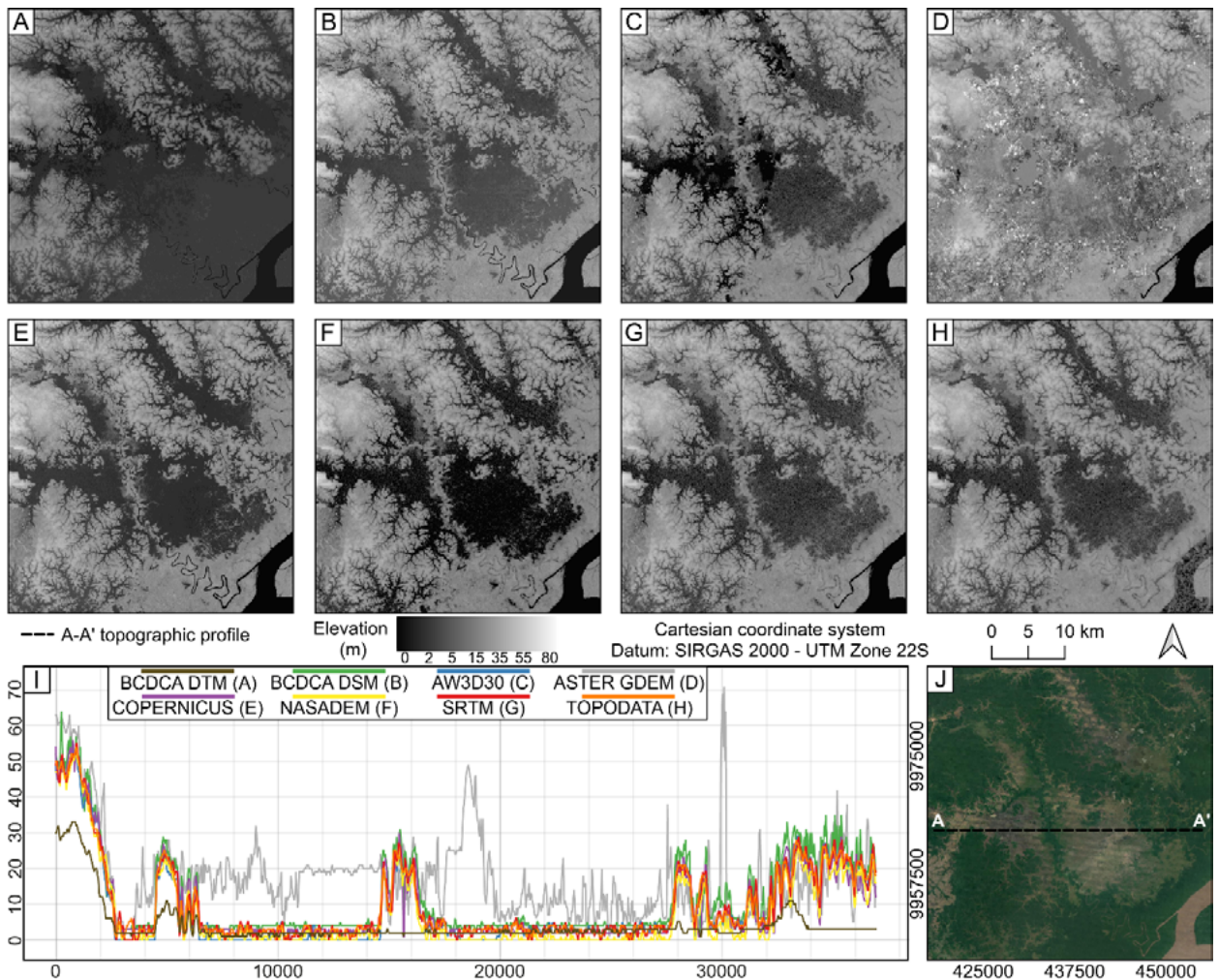

Figure 5: Hypsometry of each DEM for the study area, where: A) BCDCA DTM; B) BCDCA DSM; C) AW3D30; D) ASTER GDEM; E) Copernicus; F) NASADEM; G) SRTM; H) Topodata; I) A-A' Topographic profile and J) Visualization of A-A' profile on satellite images © Maxar Technologies, available on Google Earth Pro.

The Copernicus DEM (Figure 5E), showed a low presence of artifacts, especially in the lowland areas with low vegetation cover or bare soil. Among the DEMs natively available with a 30 m spatial resolution, Copernicus is the only one capable of representing the main larger watercourses (Amazon, Maracá-pacu and Preto rivers), an important factor especially for automated drainage network extraction. As this is the product generated from the most recent data, it is expected that the information about vegetation height and other modifications above the terrain are closer to the current reality. On the contrary, SRTM (Figure 5G), NASADEM (Figure 5F) and Topodata (Figure 5H), present few visible divergences between them, but are based on the same dataset acquired almost 15 years earlier (2000). Some divergences do appear, mainly in Topodata, where the kriging processing generates variations in areas where elevation should remain constant (horizontal), even in large water bodies like the Amazon River, due to the absence of water masks. Another difference is the noise reduction of NASADEM. The A-A' topographic profile shows that BCDCA DTM presents heights very close to zero, unlike the DSMs, which represent the forest canopy with point elevations up to 30 m (Figure 5I).

Another way to analyze the shape realism is the visual comparison of shading (Polidori and El Hage 2020), performed in a representative lowland at the study area. In this example, unlike mountainous regions where the vegetation tends to follow the contours of the terrain, BCDCA DTM maintains a flat aspect (Figure 6A), while in the DSMs, a dense and diverse vegetation is noticeable. Through the topographical profile alone (Figure 6I), the cause for this abrupt variation is unclear. Optical images show that this difference is related to different vegetation species, i.e., shrubland with height up to 10 m (brown coloration) and a transition between lowland (height up to 20 m) and upland forest (height up to 40 m), shown in the image by the variation from light green to dark green colors, respectively (Figure 6J).
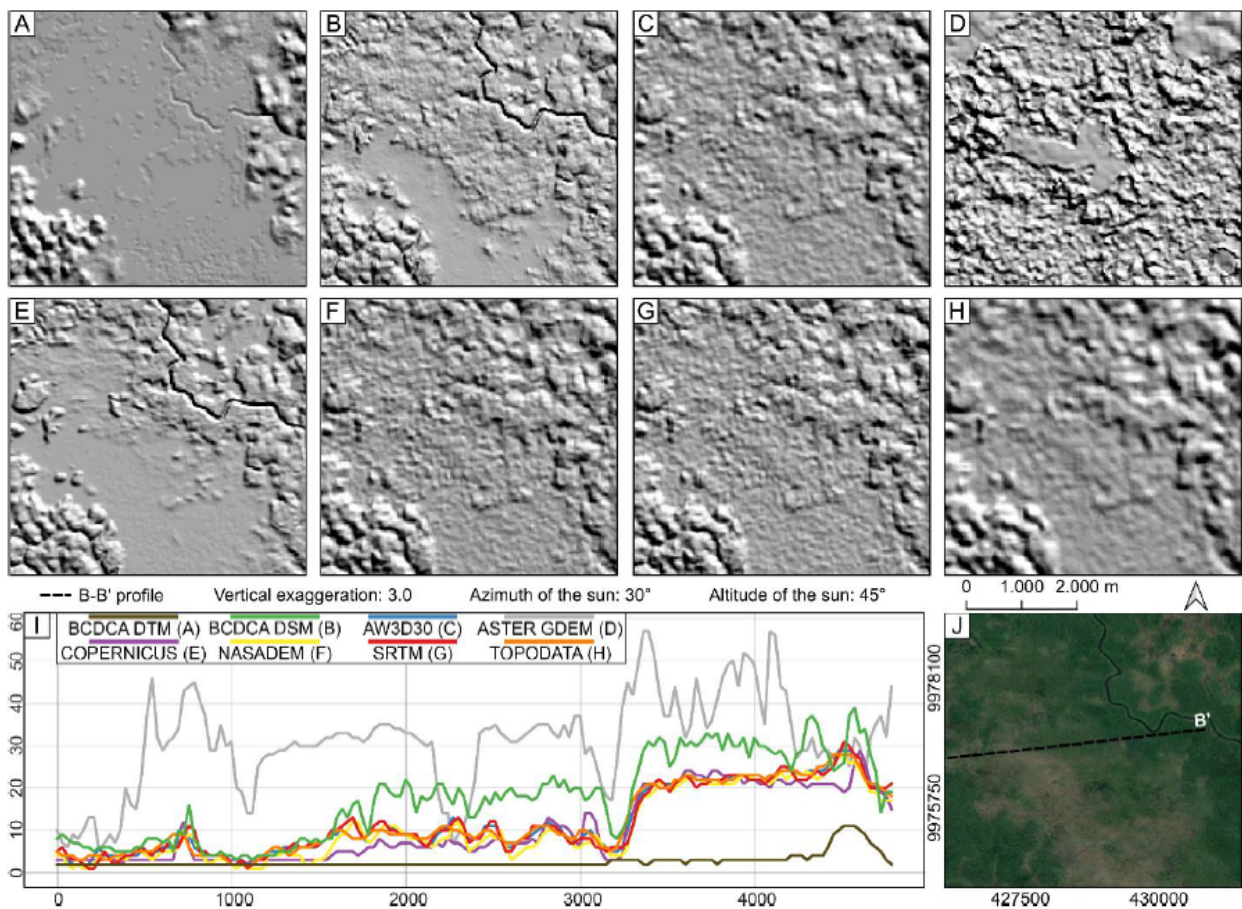

Figure 6: Shaded relief of a lowland region in the study area, where: A) BCDCA DTM; B) BCDCA DSM; C) AW3D30; D) ASTER GDEM; E) Copernicus; F) NASADEM; G) SRTM; H) Topodata; I) Final section of B-B' Topographic profile; and J) Satellite image of the study area with the section of B-B' topographic profile, available on Google Earth Pro – © Maxar Technologies.

The only DEMs where this transition is clear are BDCDA DSM and Copernicus (Figures 6B and 6E), while the others exhibit excessive noise, especially ASTER GDEM (Figure 6D). As for the terrain shape, the shading visualization confirms that Copernicus is the one that best preserves the morphology of the floodplains observed in BCDCA DTM. The BCDCA DSM maintains coherence with the terrain along the shrubland, but the transition to lowland forest is hidden by vegetation (Figure 6B). As in the other analyses, AW3D30 (Figure 6C), NASADEM (Figure 6F) and SRTM (Figure 6G) were the models that least allowed interpretation of the terrain below the canopy. In Topodata (Figure 6H), the noises are smoothed out, but the presence of artifacts is still noticeable.

The models were also evaluated based on their ability to automatically extract the hydrographic network (Figure 7A). The extracted networks were compared with the reference vector hydrographic network of Amapá State. Two lowland spots were selected within the study area, one in the transition with a low plateau area (Figure 7B), in which the drainages are well channelized, and the other one in a typical floodplain with very low height variations (Figure 7C). These two spots also present different types of vegetation, namely, lowland and upland forest in the first one, and in the second one, shrubland and herbaceous vegetation, which are naturally lower. All models were resampled to 30 m before the extraction, to allow a fair comparison.

Near low plateau areas, all DEMs present similar responses to the reference, with the exception of ASTER GDEM. For floodplain areas, where the terrain slope is almost zero, the algorithm forces the extraction of drainages from artifacts that do not reflect the terrain, related either to noise, to the resampling applied to some of the models, or to the vegetation cover. Even for BCDCA DTM, where the influence of noise and vegetation is reduced, the result does not completely match the reference network, a consequence of both the resampling of the product that simplified some features (from 2.5 m to 30 m), and its limited accuracy (Table 1). The correct characterization of the hydrography is of utmost importance for derived interpretations, like flood susceptibility mapping. However, in flat regions where landforms show little variation, this characterization needs field control, or, at least, a specialist's knowledge (Reis 2023).
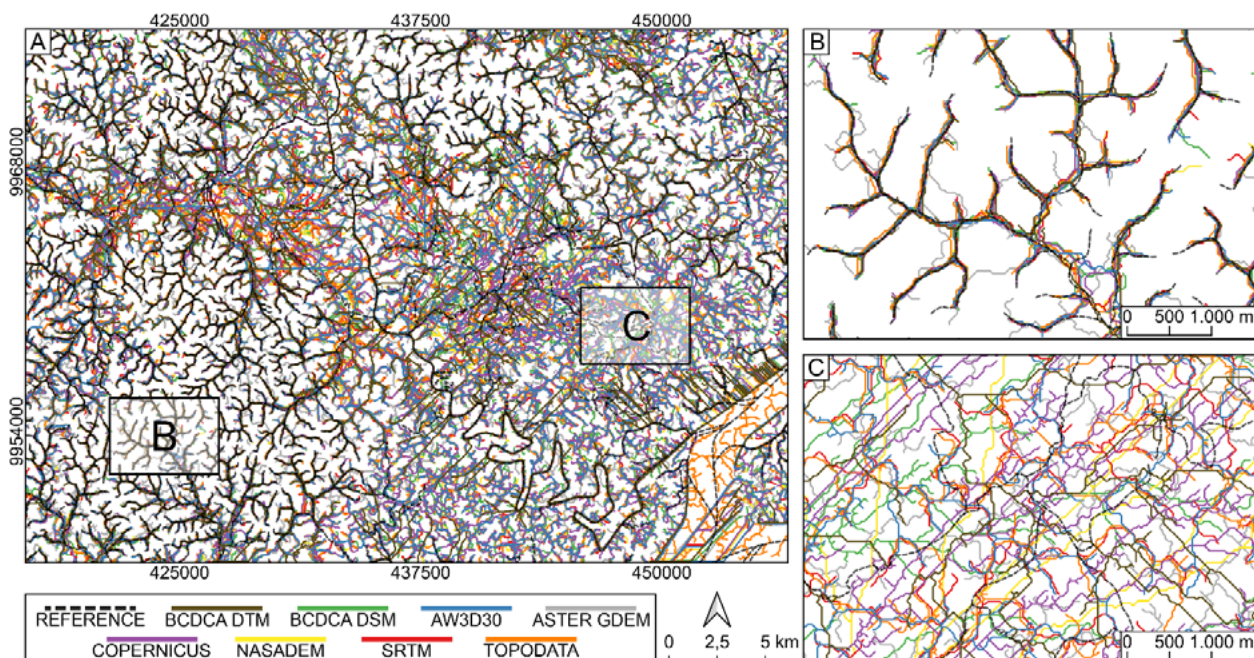

Figure 7: In A, the drainage network of the study area extracted for each of the DEM products compared to the reference hydrography; B) Low plateau area; and C) Floodplain area.

5. Discussions

5.1. Canopy effect

One of the main challenges in using DEMs for low-relief areas, as the floodplains of the Amazon coast, is the large number of non-topographic objects that the DSMs generate due to the dense vegetation cover, a characteristic defined as the "canopy effect" (Valeriano et al. 2006; Clubb et al. 2017; Polidori et al. 2018). The vegetation generates a roughness pattern that compromises not only the quality of the models in representing the surface of the terrain, but any topographic variable derived from it, such as slope and the hydrographic network extraction (Polidori, El Hage and Valeriano 2014; Zingaro et al. 2021). Both cases were observed in the results, where aside from BCDCA DTM, all DEMs were unable to predict slope and flow directions correctly (Figure 7C).

For the main global DEMs, several studies in Brazil indicate that their vertical accuracy is lower in the Amazon region than in other parts of the country, where the vegetation cover is smaller and altimetric amplitude is higher (Miceli et al. 2011; Grohmann 2018; Orlandi et al. 2019; Santos Filho et al. 2022). The main limitations of these models in forested areas are the fact that they are generated by short wavelength radar (i.e., X-band and C-band), where the radar signal is not capable of reaching the ground and the radar phase is decorrelated by the foliage movement between two acquisitions in repeat pass interferometry (Polidori et al. 2018).

Furthermore, the results indicated that apart from Topodata (Figure 6H, which was generated by kriging in order to preserve the angular features of the terrain (Valeriano and Rossetti 2012), the Copernicus DEM was the one that best preserved the geomorphological characteristics of the floodplains in the visual comparison, since it presents a lower level of roughness (Figure 6E). Using a similar criterion, Bielski et al. (2024) also came to the same conclusion in an analysis of different DEMs on a global scale, not only in the better performance of Copernicus when compared to a DTM, but also in the limitation shown by ASTER GDEM and AW3D30 compared to the other DSMs.

5.2 Scale effect

Although the results in this work are presented in a same 30 m mesh size, changes in scale can modify the geomorphological description of the terrain, as illustrated in Figure 8, where the B-B′ profile is subsampled with an increasing mesh size for all the DEMs. For elevation (Figure 8A, 8B and 8C), increasing the mesh size does not significantly affect the elevation values, it softens the noise generated by the canopy and makes the surface models more similar to the shape of the terrain (Reis 2023). The 30 m mesh Topodata presents greater consistency with the DTM when compared to SRTM and NASADEM models, since angular properties are smoothed (Valeriano and Rossetti 2012; Polidori, El Hage and Valeriano 2014). As for AW3D30, at least for the sample area of the profile, it showed much similarity with the SRTM and NASADEM models.

For slope, the effect is almost the opposite. At the 30 m mesh, the DEMs do not show a significant relationship, as the canopy effect and the artifacts resulting from the different generation techniques are clearly visible. As the mesh is degraded, the DSMs begin to show similarities with DTM in terms of slope (Figure 8E). Although resolution degradation has removed the smallest terrain shapes, slope calculation and geomorphological interpretation become reliable in DSMs, except with ASTER GDEM. However, it is noticeable that the increase in mesh size induces the disappearance of steep slopes, with slopes close to zero at the 480 m mesh (Figure 8F).

The use of high spatial resolution DEMs needs to be assessed on a case-by-case basis. BCDCA DTM and BCDCA DSM, that originally have a 2.5 m grid, can be used as examples, since even on a 30 m mesh, BCDCA DSM showed

much more roughness in the visual comparison results than the other DSMs, which indicates that on the 2.5 m mesh this would be aggravated. Nevertheless, the use of Lidar and high-resolution DTMs (such as the BCDCA DTM 2.5 m mesh) are more suitable for representing floodplains at larger scales, since the canopy effect is attenuated (Colby and Dobson 2010; Clubb et al. 2017; Santos Filho et al. 2022; Bielski et al. 2024). This effect confirms the importance of not only specifying the DEM surface (whether a DTM or a DSM) but indicate its scale for a better understand of the limitations and what expect when using it.
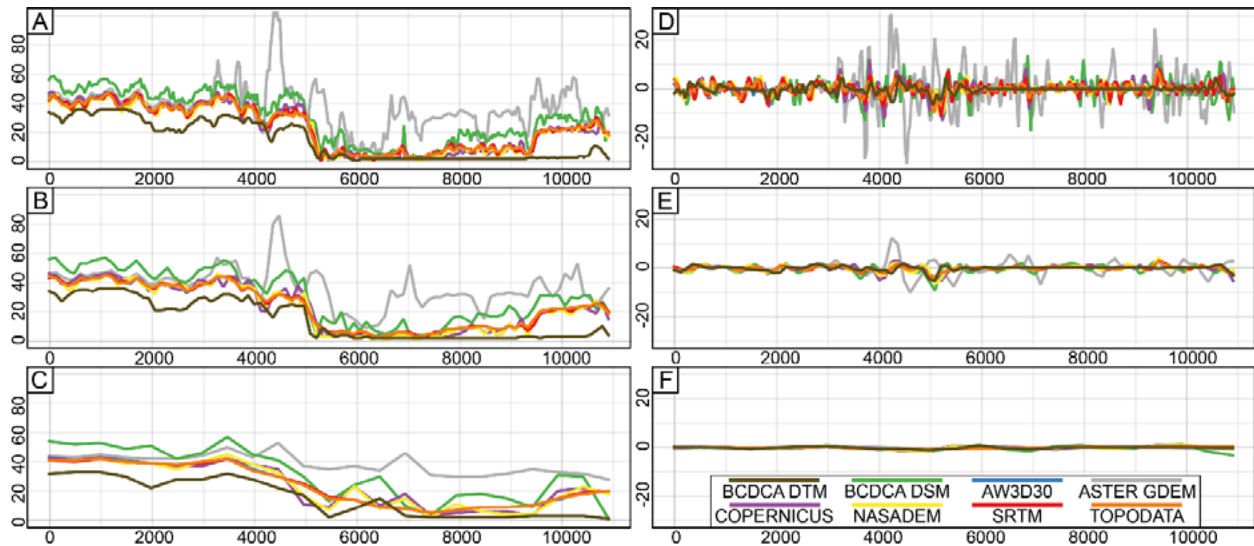

Figure 8: B-B' profile, for an area of moderate elevation in transition to lowland. On the left, the effect of resampling on elevation on mesh sizes of: A) 30 m, B) 120 m and C) 480 m. On the right, the effect of resampling on slope on meshes of: D) 30 m, E) 120 m and F) 480 m.

5.3 Temporal aspects

The current landscape of the study area is marked by the action of several natural forces, responsible for the evolution of old fluvial systems, structured along the recent geological past. Its morphology is conditioned to climatological and oceanographic dynamics and its coastal plain is seasonally flooded according to the flood regime of rivers and to semidiurnal macrotides, managed by bimodal variations of the precipitation regime in ITCZ (Santos 2006). According to Silveira (1998) the meanders along the coastal plain were active during the last Holocene Transgression (about 7,000 years ago) and its plains were directly connected to the Amazon and had a strong influence of this river until about 5,000 years.

With the lowering of the sea level, the sedimentation that gave rise to the present substrate of the floodplain forests closed these river systems (Silveira 1998; Santos 2016). Swamps were formed, occupying the landscape, and originating the present floodable fields, so that this unit would have started its formation approximately 4,700 years ago (Santos 2016). Added to the natural dynamics of the region, buffalo farming is the main anthropic intervention in the morphology of this environment. In addition to space consumption for grazing, resting and bathing of these animals, the movement of livestock favors the opening of pits that are easily confused with drainage networks in remote sensing images (Santos et al. 2008).

Considering the impact and speed of these modifications, especially those that have occurred in the last two decades, a limitation of this work is that DEMs made on different periods are compared (Table 1). The differences observed between them can lead to false interpretations of the DEM production methods, when in fact they are caused by changes in land use and cover. Furthermore, DEMs generated by photogrammetry can have important

errors if the stereoscopic pair is not of a single date, as it happens when the orbital configuration and the presence of clouds require an important waiting time of several months or years, to acquire the second image. Unlike SRTM mission products, whose data were processed from simultaneous acquisitions made with 2 antennas, ASTER GDEM and AW3D30 were obtained by automatic correlation between multiple optical images from different dates, over a landscape where the hydrography may have changed according to precipitation and other natural dynamics. This may have an important contribution to the errors observed here.

5.4 Improvement Strategies

The results confirm the challenge of relief modeling in flatlands, such as the floodplains of ACZ. The impact of vegetation, the different sources of error in height calculation and the resampling methods may be more important than the altimetric amplitude in those areas. P-band radar, that have shown to be more faithful to the terrain representation, can also fail to describe the topography in lowland areas. Due to the limitations observed in the study, the existing techniques, such as photogrammetry and InSAR, can be implemented with more abundant data or with improvement in spatial resolution, however, such solutions imply an increase in cost and time, while most users tend to make use of global and free solutions. Therefore, the burden of describing the terrain in detail to better meet users' needs should not be placed on only one technique, and improvement strategies must be applied in each specific case.

The limitation of a DTM can be compensated with the contribution of other databases, where drainage lines are represented by 2D data with more reliable geometric and topological properties (Figure 9B; Reis 2023). The use of optical images, more intuitive in describing objects than radar images, can also be an alternative, though limited by the cloudiness of the region (Figure 9C). This principle can be extended to the case where there is no river, but a slight depression that first fills when it rains. This drainage does not appear in maps and a DEM may not be accurate enough to extract its lines, but the images used to produce the DEM are sensitive to its presence. If an area is a few centimeters lower, the ground is flooded for a longer period, and therefore, it may host different plant species that are distinguished by their response, texture and spatial organization, creating recognizable color patterns in the image, which act as contour lines, i.e., tracers of the relief (Figures 6J and 9C). This possibility shows that the limitations of the DEM in flatlands, accentuated in the Amazon due to cloudiness and dense vegetation cover, can be compensated by the availability of other sources of information, as well as field measurements for validation.
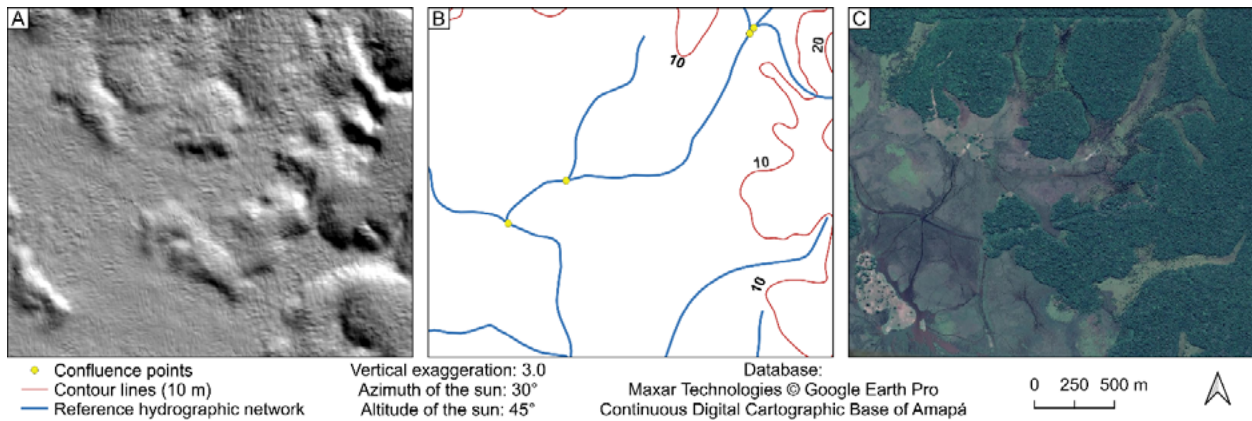
Figure 9: Floodplain in the study area, where: A) Shading visualization of BCDCA DTM; B) Vector data from BCDCA; and C) Optical images © Maxar Technologies, available on Google Earth Pro.

6. Conclusions

The analysis of eight DEMs resampled at 30 m showed that topographic mapping is a major challenge in flatlands, especially in the Amazon coast, where all techniques are potentially affected by cloudiness, a dense forest cover and flooding periods. Indeed, vegetation and others sources of error in elevation calculation and resampling can have a greater effect than natural variations in the terrain topography. A comparison of these DEMs, based on different criteria related to elevation, slope and the hydrographic network, shows that the DEM obtained from P-band radar images (BCDCA DTM) is more consistent with the landforms, as it is less sensitive to vegetation. The network automatically extracted from these models, compared to a 2D reference map, is well positioned in the hilly areas for all models, except for ASTER GDEM, while it is impossible to be positioned in the plains. This suggests alternative solutions including the use of external sources of information, such as vector data or optical imagery. The results obtained are highly scale-dependent, especially for slope-based terrain analysis, and they are limited by the landscape changes between the dates of the different DEMs. Future studies may also include field measurements for further validation of this analysis. This work provides a better understanding of the limitations of different DEMs in flatlands, especially in the humid tropics, and proposes strategies to improve the relief modeling of regions of similar complexity in a simple way.

ACKNOWLEDGEMENT

AUTHOR´S CONTRIBUTION

All authors contributed equally.

REFERENCES

Amapá State Environment Secretariat (SEMA-AP). 2015. Projeto Base Cartográfica Digital Contínua do Estado do Amapá: Especificações das Imagens SAR. Available at: <https://sema.portal.ap.gov.br/conteudo/servicos-e-informacoes/base-cartografica>. [Accessed 11 October 2020].

Azevedo, L. 1971. Radar in the Amazon. *Proceedings of the 7th International Symposium on Remote Sensing of Environment*, 3, pp.2303-2306.

Bielski, C. et al. 2024. Novel approach for ranking DEMs: Copernicus DEM improves one arc second open global topography. *IEEE Transactions on Geoscience & Remote Sensing*, 62, pp.1-22.

Buckley, S.M. et al. 2020. NASADEM User Guide. NASA JPL; Pasadena, CA, USA, 52p.

Clubb, F. J. et al. 2017. Geomorphometric delineation of floodplains and terraces from objectively defined topographic thresholds. *Earth Surface Dynamics*, 5(3), pp.369-385.

Colby, J. D. and Dobson, J. G. 2010. Flood Modeling in the Coastal Plains and Mountains: Analysis of Terrain Resolution. *Natural Hazards Review*, 11(1), pp.19-28.

Farr, T. G. et al. 2007. The Shuttle Radar Topography Mission. *Review of Geophysics*, 45, RG2004.

GRASS Development Team. 2022. Geographic Resources Analysis Support System (GRASS GIS) Software, Version 7.8.7. Available at: <http://grass.osgeo.org> [Accessed 15 September 2020].

Grohmann, C. H. 2018. Evaluation of TanDEM-X DEMs on selected Brazilian sites: Comparison with SRTM, ASTER GDEM and ALOS AW3D30. *Remote Sensing of Environment*. 212, pp.121-133.

Guth, P. L. et al. 2021. Digital Elevation Models: Terminology and Definitions. *Remote Sensing*, 13(18), 3581.

Hayakawa, Y. S. Oguchi, T. and Lin, Z. 2008. Comparison of new and existing global digital elevation models: ASTER G-DEM and SRTM-3. *Geophysical Research Letters*, 35, L17404.

Holmgren, P. 1994. Multiple flow direction algorithms for runoff modelling in grid-based elevation models: An empirical evaluation. *Hydrological Processes*, 8(4), pp.327-334.

Leister-Taylor, V. et al. 2020. *Copernicus Digital Elevation Model Product Handbook*. Tech. Rep. GEO.2018-1988-2, AIRBUS.

Miceli, B. S. et al. 2011. Avaliação vertical de modelos digitais de elevação (MDEs) em diferentes configurações topográficas para médias e pequenas escalas. *Revista Brasileira de Cartografia*. 63(1), pp.191-201.

Nittrouer, C. A. Brunskill, G. J. and Figueiredo, A. G. 1995. Importance of tropical coastal environments. *Geo-Marine Letters*, 15: pp.121-126.

Orlandi, A. G. et al. 2019. Vertical accuracy assessment of the processed SRTM data for the Brazilian territory. *Bulletin of Geodetic Sciences*. 25(4): pp.1-14.

Pereira, L. C. C. et al. 2009. A zona costeira amazônica. *Journal of Integrated Coastal Zone Management*, 9(2), pp.3-7.

Pham, H. T. et al. 2018. A method for combining SRTM DEM and ASTER GDEM2 to improve topography estimation in regions without reference data. *Remote Sensing of Environment,* 210, pp.229-241.

Polidori, L. El Hage, M. and Valeriano, M. D. M. 2014. Digital elevation model validation with no ground control: Application to the Topodata DEM in Brazil. *Bulletin of Geodetic Sciences*, 20, pp.467–479.

Polidori, L. et al. 2018. Potential of P-Band SAR Topographic products over forested areas in terms of terrain morphological description: A preliminary study in the framework of the Biomass Mission. *Proceedings of the Simposio Latinoamericano Percepción Remota y Sistemas de Información Espacial*, Havana, Cuba, pp.6-9.

Polidori, L. and El Hage, M. 2020. Digital elevation model quality assessment methods: A critical review. *Remote Sensing*. 12(21), 3522.

QGIS Development Team. 2022. QGIS Geographic Information System Version 3.22.5. Open-Source Geospatial Foundation. Available at: <http://qgis.osgeo.org> [Accessed 17 September 2020].

Rabelo, B. V. ed. 2008. *Macrodiagnóstico do Estado do Amapá primeira aproximação do ZEE*. 3. ed. Macapá: IEPA-COT-ZEE. 139 p.

Reis, L. N. 2023. *Caracterização morfológica de planícies inundáveis na costa do Amapá: uma análise a partir de modelos digitais de elevação*. Masters dissertation. Universidade Federal do Pará, Instituto de Geociências, Programa de Pós-Graduação em Geologia e Geoquímica, Belém.

Santos Filho, H. et al. 2022. Cartographic Accuracy Standard (CAS) of the digital terrain model of the digital and continuous cartographic base of the state of Amapá: case study in the city of Macapá. *Bulletin of Geodetic Sciences*, 28(3), pp.1-20.

Santos, V. F. D. 2006. *Ambientes Costeiros Amazônicos. Avaliação de modificações por sensoriamento remoto*. PhD. Universidade Federal Fluminense, Instituto de Geociências, Programa de Pós-Graduação em Geologia e Geofísica Marinha, Niterói.

Santos, V. F. D. 2016. Dinâmica de inundação em áreas úmidas costeiras: zona urbana de Macapá e Santana, costa amazônica, Amapá. *Revista Eletrônica de Humanidades do Curso de Ciências Sociais da UNIFAP*, 9, pp.121-144.

Santos, V. F. D. et al. 2008. Aplicação de dados multisensor (SAR e ETM+) no reconhecimento de padrões de uso e ocupação do solo em costas tropicais: Costa amazônica, Amapá, Brasil. *Revista Brasileira de Geofísica*, 27, pp.39-55.

Silveira, O. F. M. D. 1998. *A planície costeira do Amapá: dinâmica de ambiente costeiro influenciado por grandes fontes fluviais quaternárias*. PhD. Universidade Federal do Pará, Centro de Geociências, Programa de Pós-Graduação em Geologia e Geoquímica, Belém.

Silveira, O. F. M. D. and Santos, V. F. D. 2006. *Aspectos Geológicos-Geomorfológicos Região Costeira Entre o Rio Amapá Grande e a Região dos Lagos do Amapá*. MMA/PROBIO, Macapá.

Souza, E. B. and Cunha, A. C. 2010. Climatologia de Precipitação no Amapá e mecanismos climáticos de grande escala. In: Cunha, A.C. Souza, E. B. Cunha, H.F.A. ed. *Tempo, Clima e Recursos Hídricos: Resultados do projeto REMETAP no estado do Amapá*. Macapá: IEPA, 2010. pp.177-195.

Souza Filho, P. W. M. et al. 2005. Sistemas de observação costeira e o papel dos sensores remotos no monitoramento da costa norte brasileira, Amazônia. *Revista Brasileira de Cartografia*, 57(2), pp.79-86.

Tachikawa, T. et al. 2011. Characteristics of ASTER GDEM version 2. *IEEE International Geoscience and Remote Sensing Symposium*, pp.3657–3660.

Takaku, J. et al. 2014. Generation of high-resolution global DSM from ALOS PRISM. *International Archives of the Photogrammetry, Remote Sensing and Spatial Information Sciences*, 4, pp.243–248.

Torres, A. M. and El-Robrini, M. 2006. Amapá. In: Muehe, D. ed. 2006. *Erosão e Progradação do litoral Brasileiro*. Brasília: M.M.A.

Valeriano, M. M. et al. 2006. Modeling small watersheds in Brazilian Amazônia with SRTM-90 m data. *Computers and Geosciences*, 32, pp.1169-1181.

Valeriano, M. M. and Rossetti, D. F. 2012. Topodata: Brazilian full coverage refinement of SRTM data. *Applied Geography*, 32, pp.300-309.

Van Roessel, J. W. and Godoy, R. C. 1974. SLAR Mosaics for Project RADAM. *Photogrametric Engineering,* 40(5), pp.583-595.

Vieira, M. S. 2015. Base cartográfica contínua do estado do Amapá. *Revista Digital Simonsen*, 1(3), pp.47-61.

Wehr, A. and Lohr, U. 1999. Airborne laser scanning—an introduction and overview. *ISPRS Journal of Photogrammetry and Remote Sensing*, 54(2–3), pp.68-82.

Zebker, H. A. and Goldstein, R. M. 1986. Topographic mapping from interferometric SAR observations. *Journal of Geophysical Research*, 91: pp.4993-4999.

Zingaro, M. et al. 2021. Suitability assessment of global, continental and national digital elevation models for geomorphological analyses in Italy. *Transactions in GIS*, 00, pp.1–26.